Non-iterative Multi-modal Partial View to Full View Image Registration Using Local Phase-Based Image Projections

Ilker Hacihaliloglu[1], David R. Wilson[1], Michael Gilbart[1], Michael Hunt[2], and Purang Abolmaesumi[3]

[1] Departments of Orthopaedics
[2] Physical Therapy
[3] Electrical and Computer Engineering
University of British Columbia, Vancouver, BC, Canada
purang@ece.ubc.ca

Abstract. Accurate registration of patient anatomy, obtained from intra-operative ultrasound (US) and preoperative computed tomography (CT) images, is an essential step to a successful US-guided computer assisted orthopaedic surgery (CAOS). Most state-of-the-art registration methods in CAOS require either significant manual interaction from the user or are not robust to the typical US artifacts. Furthermore, one of the major stumbling blocks facing existing methods is the requirement of an optimization procedure during the registration, which is time consuming and generally breaks when the initial misalignment between the two registering data sets is large. Finally, due to the limited field of view of US imaging, obtaining scans of the full anatomy is problematic, which causes difficulties during registration. In this paper, we present a new method that registers local phase-based bone features in frequency domain using image projections calculated from three-dimensional (3D) radon transform. The method is fully automatic, non-iterative, and requires no initial alignment between the two registering datasets. We also show the method's capability in registering partial view US data to full view CT data. Experiments, carried out on a phantom and six clinical pelvis scans, show an average 0.8 mm root-mean-square registration error.

Keywords: 3D ultrasound, CT, registration, local phase, radon transform, non-iterative, phase correlation, computer assisted orthopaedic surgery.

1 Introduction

With the recent advances made in imaging technology and instrumentation, image-guided interventions have been extended to address clinical problems in various orthopaedic surgical procedures such as pedicle screw placement [1], total hip arthroplasty [2], and shoulder arthoscopy [3]. In recent years, given the concerns due to high ionizing radiation of intra-operative X-ray fluoroscopy, US imaging has been

P. Abolmaesumi et al. (Eds.): IPCAI 2012, LNAI 7330, pp. 64–73, 2012.

proposed as an intra-operative imaging modality to assist with these surgical procedures. US is a real-time, inexpensive and non-ionizing imaging modality. However, US imaging has several limitations including user dependent image acquisition, limited field of view, and low signal to noise ratio (SNR). In particular to orthopaedic surgical procedures, the appearance of bone surfaces in US remains strongly influenced by the beam direction, and regions corresponding to bone boundaries appear blurry [4]. In order to alleviate some of these difficulties, pre-procedure data obtained from other imaging modalities, such as CT and MRI, have been registered with US scans. The ability to perform this registration accurately, automatically, and rapidly is critical for enabling more effective US-guided procedures in CAOS.

Since the first introduction of computer assisted surgery (CAS) a number of image registration methods have been developed. Specifically for orthopaedic surgery, due to the rigid nature of bone anatomy, surface-based registration methods have gained popularity [5]. Penney et al. [5] improved the robustness of the standard ICP by randomly perturbing the point cloud positions, which allowed the algorithm to move out of some local minima and find a minimum with lower residual error. The method was validated on a phantom femur data set where a mean target registration error (TRE) of 1.17 mm was achieved. The main drawback in that method remained the manual extraction of bone surfaces from US data. Moghari and Abolmaesumi [6] proposed a point-based registration method based on Unscented Kalman Filter (UKF). Although the method improved the registration speed, accuracy and robustness compared to standard ICP the main drawback was the extraction of bone surfaces from US images, which was done manually. Recently, Brounstein et al. [7] proposed a Gaussian Mixture Model (GMM) based surface registration algorithm, where the bone surface was extracted automatically from both modalities. The root mean square distance between the registered surfaces was reported to be 0.49 mm for phantom pelvis data and 0.63 mm for clinical pelvis data.

In order to avoid the segmentation of bone surfaces from US data, intensity-based registration methods have been developed. Brendel et al. [8] proposed a surface to volume registration method. They preprocess the CT data by segmenting only the bone surfaces that could be visible in the US using the US imaging probe orientation information. These extracted bone surfaces were then registered to the B-mode US data by maximizing the sum of the overlapping gray values of pre-processed CT bone surfaces and US data. While this method showed accurate registration results, it assumed a known probe orientation for pre-processing the CT data. This assumption may not necessarily be valid, especially for fracture reduction surgeries where the US probe needs to be realigned after a fracture reduction. Penney et al. [9] used normalized cross-correlation similarity metric to register bone probability images obtained from CT and US data sets using intensity, gradient, and US shadowing artifact information. Successful registration results were reported; however, generation of US probability images depended on segmentation information obtained from several prior data sets. Gill et al. [10] simulated US images from CT data for registering bone surfaces of the spine and achieved a registration accuracy of 1.44 mm for phantom scans and 1.25 mm for sheep cadaver scans. In a recent publication, ultrasound image simulation was performed on statistical shape models [11] where a TRE less than 3 mm was reported. In order to achieve clinically acceptable

registration results this technique required accurate initial alignment of the SSM and three-dimensional (3D) US data.

Most of the previously proposed US-CT registration methods either require manual interaction for segmenting bones from US images or for initial registration to bring the two surfaces closer [5-7]. Several groups have proposed methods, based on intensity and gradient information, to automate the bone segmentation process [12]. However, due to the typical US artefacts there methods remain highly sensitive to parameters settings and have been mainly limited to 2D US data. Furthermore, one of the major stumbling blocks facing all of the proposed registration methods is the requirement of an iterative optimization procedure during the registration, which is time consuming and normally does not converge if the misalignment between the two registering data sets is large. Finally, due to the limited field of view of US imaging, obtaining scans of the full anatomy is problematic which causes difficulties during the registration.

In this paper, we present a registration method that estimates the 3D rotation and translation parameters, between the CT and US volumes, in frequency domain using local phase-based image projections. The method is fully automatic, non-iterative, and requires no initial alignment between the two datasets. We also show the method's capability in registering partial view US data to full view CT data. We validate the method on pelvic scans obtain from a phantom setup as well as six clinical scans.

2 Materials and Methods

2.1 Local Phase Based Bone Surface Extraction

Hacihaliloglu et al. [13] recently proposed a method that uses 3D local phase information to extract bone surfaces from 3D US data. The local phase information is extracted by multiplying the US volumes in frequency domain with the transfer function of 3D Log-Gabor filter (*3DLG*):

$$3DLG(p,\omega,\theta,\phi,\omega_0,\theta_{\mathrm{I}},\phi_{\mathrm{i}}) = \exp\left(-\frac{\left(\log\left(\frac{\omega}{\omega_0}\right)\right)^2}{2\left(\log\left(\frac{\kappa}{\omega_0}\right)^2\right)}\right) \times \exp\left(-\frac{\alpha(\mathrm{p},\theta_{\mathrm{I}},\phi_{\mathrm{i}})^2}{2\sigma_\alpha^2}\right). \quad (1)$$

Here, κ is a scaling factor used to set the bandwidth of the filter in the radial direction, and ω_0 is the filter's center spatial frequency. To achieve constant shape-ratio filters, which are geometric scalings of the reference filter, the term κ/ω_0 must be kept constant. The angle between the direction of the filter, which is determined by the azimuth (ϕ) and elevation (θ) angles, and the position vector of a given point p in the frequency domain expressed in Cartesian coordinates in the spectral domain is given by $\alpha(p, \phi_i, \theta_i) = arcos(p \times v_i / \|p\|)$, where $v_i = (cos\phi_i \times cos\theta_i, cos\phi_i \times sin\theta_i, sin\phi_i)$ is a unit vector in the filter's direction and σ_α is the standard deviation of the Gaussian function in the angular direction that describes the filter's angular selectivity. To obtain higher orientation selectivity, the angular function needs to be narrower. The scaling of the radial Log-Gabor function is controlled using different wavelengths that are based on multiples of a minimum wavelength, λ_{min}, a user-defined parameter. The filter scale m, and center frequency ω_0 are related as $\omega_0 = 2/\lambda_{min} \times (\delta)^{m-1}$ where δ is a scaling factor

defined for computing the center frequencies of successive filters. By using the above 3D filter over a number of scales (m) and at different orientations (i), a 3D phase symmetry (PS) measure can then defined as in (2):

$$PS_{3D}(x,y,z) = \frac{\sum_i \sum_m \lfloor [|e_{im}(x,y,z)| - |o_{im}(x,y,z)|] - T_i \rfloor}{\sum_i \sum_m \sqrt{e_{im}^2(x,y,z) + o_{im}^2(x,y,z)} + \varepsilon}. \quad (2)$$

The even and odd components, $e_{im}(x, y, z)$ and $o_{im}(x, y, z)$, of *3DLG* are calculated using the real and imaginary responses of the Log-Gabor filter for each voxel point (x, y, z). T_i is a threshold to account for noise in the US image and ε is a small number to avoid division by zero [13]. Using this method local phase bone surfaces were extracted from both US and CT data set, which are denoted as PS_{3DCT} and PS_{3DUS} from this point on. Since US imaging modality can only image the top surface of bone ray casting is applied to the local phase bone surface extracted from CT volume set leaving only the top surface of the bone that could be imaged with US. These two local phase bone surfaces are used as input to the next step.

2.2 Local Phase Projection Space from 3D Radon Transform

Bone responses in B-mode US images typically appear as elongated line-like objects with higher intensity values compared to the other image features. Integrating the intensity values along these bone responses in an image will produce a higher value than doing the integration along a non-bone response (Fig. 1). Based on this simple idea, we propose to use the 3D Radon Transform (*3DRT*) in order to detect the orientation and location of the bone surfaces. *3DRT* represents a 3D volume as a collection of projections in a function domain $f(x,y,z)$ along various planes defined by the shortest distance ρ from origin, the angle azimuth ϕ around z axis and the angle of elevation θ around the y axis:

$$3DRT(\rho,\emptyset,\theta) = \int\int\int f(x,y,z)\delta(\rho - xcos\emptyset cos\theta - ysin\emptyset sin\theta - zsin\theta)dxdydz. \quad (3)$$

The *3DRT* is calculated for the local phase bone surface points extracted in 2.1. From this point on the *3DRT* volumes will be denoted as $3DRT_{CT}(\rho_{CT},\phi_{CT},\theta_{CT})$ and $3DRT_{US}(\rho_{US},\phi_{US},\theta_{US})$ for the CT and US bone surfaces, respectively.

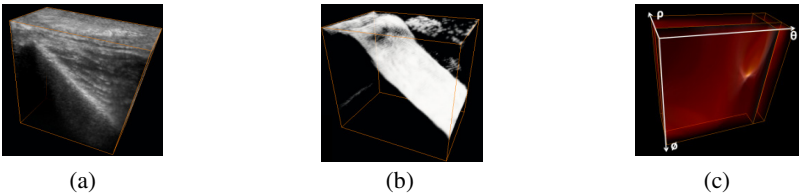

(a) (b) (c)

Fig. 1. 3D Radon Transform (3DRT) and bone orientation estimation. (a) B-mode US volume; (b) 3D phase symmetry volume of (a); (c) 3DRT of (b) where the high intensity region is showing a peak (high intensity) in the 3DRT space due to integration of the bone surface for the angle values that are corresponding to the bone surface orientation.

2.3 Projection Based Phase Correlation for CT-US Registration

The *3DRT*s calculated in Section 2.2 are used as the input volumes to the phase correlation based registration method. The rigid body registration problem is solved in two steps: first estimating the 3D rotation, then the 3D translation. In order to calculate the angle difference in the azimuth direction (z axis) between the $3DRT_{CT}$ and $3DRT_{US}$ volumes, intensity values along the elevation direction (y axis) are summed resulting in two-dimensional (2D) RT images denoted as $2DRT_{CTy}$ (ρ_{CT},ϕ_{CT}) and $2DRT_{USy}$ (ρ_{US},ϕ_{US}), respectively. From properties of RT the relationship between these two RT images is given by:

$$2DRT_{CTy}(\rho_{CT},\emptyset_{CT}) = 2DRT_{USy}((\rho_{CT} - \Delta\rho_{\emptyset},\emptyset_{CT} - \emptyset). \tag{4}$$

Here, $\Delta\rho_{\phi}=(\Delta x^2+ \Delta y^2)^{0.5}\times sin(\phi\text{-}tan^{-1}(\Delta x /\Delta y))$ where $(\Delta x ,\Delta y)$ is the translational difference in x and y directions. Let $F_{CTy}(f,\phi_{CT})$ and $F_{USy}(f,\phi_{US})$ denote the one-dimensional (1D) Fourier transforms with respect to the first argument of $2DRT_{CTy}$ and $2DRT_{USy}$, respectively. For each ϕ_{CT},ϕ_{US} angle combination a projection based phase correlation function is calculated.

$$PC_{rot}(\emptyset_{CT},\emptyset_{US}) = \frac{F_{CTy}(f,\emptyset_{CT}) \times F^{*}_{USy}(f,\emptyset_{US})}{\left|F_{CTy}(f,\emptyset_{CT}) \times F^{*}_{USy}(f,\emptyset_{US})\right|}. \tag{5}$$

In Equation (5), F^{*} denotes the complex conjugate. Next step involves the calculation of the $Peak(\phi_{CT},\phi_{US})=max(IF^{-1}(PC_{rot}(\phi_{CT}, \phi_{US})))$ matrix where IF^{-1}denotes the 1D inverse Fourier transform operation. The $Peak(\phi_{CT}, \phi_{US})$ matrix will have high intensity pixels when $\phi_{CT}=\phi+\phi_{US}$ since the correlation between the $2DRT_{CTy}$ and $2DRT_{USy}$ images will be high for these angles. Thus, we introduce a sum function $Sum_y(a)$:

$$\begin{aligned} Sum_y(a) &= \sum_{\emptyset} Peak(\emptyset_{CT},\emptyset_{CT} - a)\ where\ \emptyset_{CT} - a \geq 0 \\ Sum_y(a) &= \sum_{\emptyset} Peak(\emptyset_{CT},180 + \emptyset_{CT} - a)\ where\ \emptyset_{CT} - a \leq 0 \end{aligned} \tag{6}$$

Function $Sum_y(a)$ will reach a maximum value at $a=\phi$ [14]. Consequently, the rotation angle ϕ is detected by determining the maximum value of $Sum_y(a)$ [14]. After finding the ϕ angle same analysis is repeated to find the rotation difference θ in the elevation direction (y axis), this intensity summation is performed along the z axis resulting in 2D *RT* images denoted as $2DRT_{CTz}$ (ρ_{CT},ϕ_{CT}) and $2DRT_{USz}$ (ρ_{US},ϕ_{US}), respectively. The only difference is that this time the intensity summation is performed along the azimuth direction.

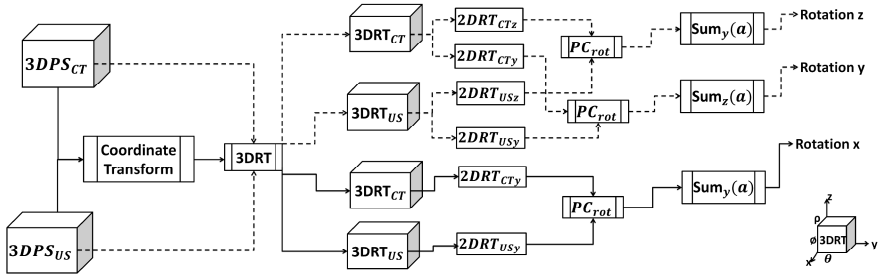

(a)

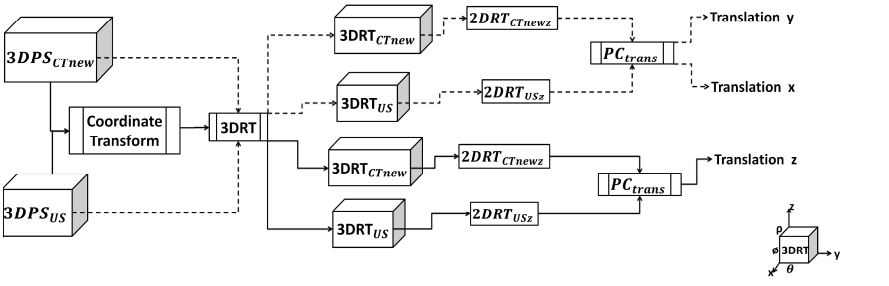

(b)

Fig. 2. Flowchart for the proposed 3D rotation (a) and translation (b) estimation

The integration in the *3DRT* given in Equation (3) is done along the *y* and *z* axis. In order to calculate the final rotation (rotation around the *x* axis), this integration has to be done around *x* axis. To achieve this a coordinate transformation is done in the original $3DRT_{US}$ and $3DRT_{CT}$ volumes making the *x* axis to be represented as the *z* axis in both volumes. Rotation *x* can now be calculated as explained previously for the elevation angle (ϕ) calculation. The 3D rotation estimation process is shown in Fig.2 (a) as a flowchart.

The calculated angle values are used to correct for the rotational difference between the PS_{3DCT} and PS_{3DUS} volumes. After this correction the only difference between the two local phase volumes is the 3D translational difference. A new *3DRT* is calculated for the rotation corrected local phase volume. Let us symbolize this new *3DRT* volume as $3DRT_{\mathrm{CT}new}$. As in the rotation estimation part the new $3DRT_{\mathrm{CTnew}}$ volume is reduced to 2D by summing the intensity values along the azimuth direction (*z* axis). This new 2D image $2DRT_{CTnezz}(\rho_{CT},\theta)$ and the previously calculated $2DRT_{USz}(\rho_{US},\theta)$ are used as inputs to the PC_{trans} formula given in Equation (7) below. The angle values in $2DRT_{USz}$ and $2DRT_{CTnewz}$ are the same stating that there is no rotational difference between these two images.

$$PC_{trans}(f,\phi) = \frac{F_{USz}(f,\theta) \times F^{*}_{CTnewz}(f,\theta)}{|F_{USz}(f,\theta) \times F^{*}_{CTnewz}(f,\theta)|}. \tag{7}$$

Again, $F_{USz}(f,\theta)$ and $F_{CTnewz}(f,\theta)$ denote the one dimensional (1D) Fourier transforms of $2DRT_{USz}$ and $2DRT_{CTnewz}$, respectively, whereas F^* denotes the complex conjugate. Next step involves the calculation 1D inverse Fourier transform of $PC_{trans}(f,\theta)$ in order to obtain $pc_{trans}(\rho,\theta)= IF^{-1}(PC_{trans}(f,\theta))$.

From Equation (4), we know that this function will have high intensity values when $\rho_{CT}=(\Delta x^2+ \Delta y^2)^{0.5}\times sin(\phi\text{-}tan^{-1}(\Delta x /\Delta y))$ since the correlation between the reference and floating images will be the highest for these ρ_{CT} values. In order to find the translational displacement in x and y directions the final step involves taking the inverse RT of $pc_{trans}(\rho,\theta)$ and searching the maximum peak value of $H(x,y)=2DRT^{-1}(pc_{trans}(\rho,\theta))$. Here, $2DRT^{-1}$ denotes the inverse RT operation. The translation in the z direction is calculated using the same method after the coordinate transformation operation to the $3DRT_{CTnew}$ and $3DRT_{US}$ volumes [14]. Fig. 2 (b) shows a simple flowchart of the 3D translation estimation method.

2.4 Data Acquisition and Experimental Setup

A Sawbones pelvis bone model (#1301, Research Laboratories, Inc., Vashon, WA) was used during the phantom validation experiment. 38 fiducial markers with 1 mm diameter were attached to the surface of the phantom specifically covering the iliac and pubic crest regions. This phantom setup was immersed inside a water tank and imaged with a GE Voluson 730 Expert Ultrasound Machine (GE Healthcare, Waukesha, WI) using a 3D RSP4-12 probe. The US phantom volumes were 152×198×148 voxels with an isometric resolution of 0.24 mm. The CT volume was taken with a Toshiba Aquilion 64 (Tustin, CA). The voxel resolution was 0.76 mm×0.76 mm×0.3 mm. The 3DRT was implemented in C++. Local phase bone surface extraction together with the registration method was implemented in Matlab (The Mathworks Inc., Natick, MA, USA). The US and CT volumes were initially aligned using the gold standard for registration calculated from fiducial markers. The CT volume was then perturbed by a random transform chosen from a uniform distribution of ±10 mm translation along each axis and ±10° rotation about each axis. In total 100 different distributions were introduced to the CT volume. The misaligned CT volumes were then registered back to the US volume using our proposed registration algorithm. Accuracy was determined by the ability of the registration to recover to the fiducial-based gold standard and is reported as the mean Target Registration Error (TRE) calculated as the misalignment of the four new fiducals, which were not included in the initial fiducial based registration. The Surface Registration Error (SRE) was calculated as the Root Mean Square (rms) distance between the registered surfaces.

Following all required ethics approvals, we also obtained both CT and US scans from consenting patients admitted to a Level 1 Trauma Centre with pelvic fractures that clinically require a CT scan. The voxel resolution for the CT volumes varied between 0.76 mm-0.83 mm in x and y axes and 1 mm-2 mm in z. The US volumes were acquired using the same US machine as described in the phantom study. In total six patients were scanned. The RMS error between the registered bone surface volumes was used for quantitative validation.

3 Results

Figure 3 shows the registration results for one of the introduced misalignments in the phantom study. During the registration process the entire left pelvis was used as the CT surface and no ROI was defined. The proposed registration method successfully aligns the two volumes where a close match between the surfaces is visible (Fig.3.). The tests on the phantom setup showed an average 2.06 mm (SD 0.59 mm) TRE with maximum TRE of 3.34 mm. The mean surface registration error for the phantom study was calculated as 0.8 mm (SD 0.62 mm).

Figure 4 shows the qualitative results obtained from the clinical study. The US scans were obtained from the healthy (unaffected by the fracture) side of the pelvis. The mean SRE, obtained from the six patients, was 0.74 (SD 0.22 mm) with maximum SRE of 1.1 mm. The runtime for the 3D RT for a 400×400×400 volume is 4 min. The MATLAB implementation of the registration method takes 2 min.

4 Discussion and Conclusion

We proposed a method for CT-US registration that is based on aligning local phase based bone features in frequency domain using their projections. Unlike the previous approaches the proposed method is fully automatic, non-iterative and requires no initial alignment between the two datasets. Using local phase images as input images to PC method eliminates the typical edge effect problem, which is one of the main problems faced in PC based registration methods. The use of RT in order to estimate the rotation proved to be very robust specifically in bone US images. During the traditional Fourier Transform based registration algorithms the rotation is estimated by transforming Cartesian coordinates to polar coordinates. During this transformation image pixels close to the center are oversampled while image pixels further away from the center are under sampled or missed, which causes problems for rotation estimation. On the other hand, RT concentrates on the image regions where high feature information is available, which makes the method more robust to rotation estimation.

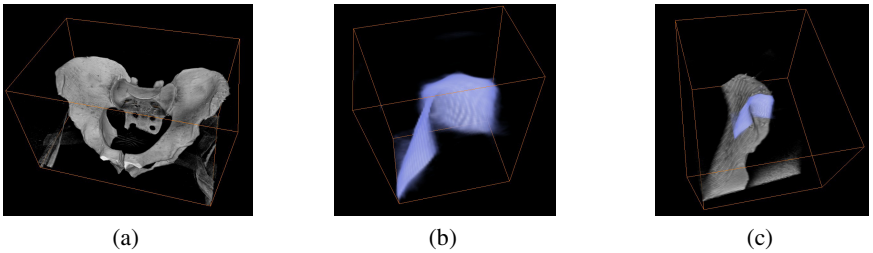

(a) (b) (c)

Fig. 3. Qualitative validation for phantom study. (a) 3D phase symmetry surface of phantom pelvis; (b) 3D local phase symmetry surface; (c) shows the obtained registration result where (a) is registered to (b). Note that the entire left pelvis is used for registration and no ROI was selected.

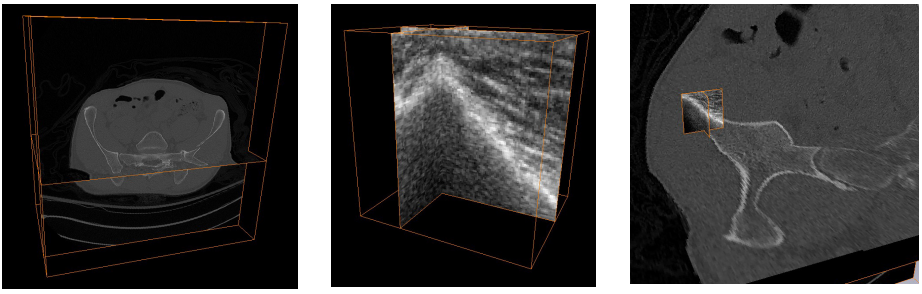

(a) (b) (c)

Fig. 4. Qualitative validation for clinical study. (a) CT data obtained from a pelvic ring fracture patient; (b) corresponding 3D US volume; (c) overlay of registration result.

The calculation of RT requires some discretization as well which could potentially introduce some errors. Recently, sparsity based image processing techniques have shown to improve the calculation of the RT [15]. This will be further investigated as a future step. Furthermore, in US based orthopaedic surgery applications the bone surfaces typically appear as elongated line-like features. This information was incorporated into the proposed framework using the traditional RT where the intensity integration was performed along a line. In order to enhance bone features or soft tissue interfaces that have a curved appearance this traditional RT could be extended to generalized RT where the integration would be performed alone a curve.

One limitation of the proposed method is its dependency on the extracted local phase features. Since US is a user dependent imaging modality the proper orientation of the US transducer plays an important role during the data collection. If the transducer is aligned properly, the bone surface will be represented with a high intensity line-like region followed by a shadowing feature which results in the accurate extraction of local phase bone surfaces. On the other hand, wrong orientation of the transducer will result in weak bone responses which will also affect the extracted local phase bone features. In these situations the proposed method could be used as an initial registration step that could be further optimized using an intensity based method followed by this initial registration.

We believe that the registration time could be reduced by implementing the method on a Graphics Processing Unit (GPU). While the registration procedure has shown promise in the tests, it still requires further improvements to the implementation and must be further validated to be ready for a clinical application. Future work will focus on reducing the registration runtime and on extensive validation of the registration technique on more clinical scans.

Acknowledgments. This work was funded by Mprime Network.

References

1. Nolte, L.P., Zamorano, L.J., Jiang, Z., Wang, Q., Langlotz, F., Berlemann, F.: Image-guided insertion of transpedicular screws. A Laboratory Set-Up. Spine 20(4), 497–500 (1995)
2. Jaramaz, B., DiGioia, A.M., Blackwell, M., Nikou, C.: Computer assisted measurement of cup placement in total hip replacement. Clinical Orthopaedics 354, 70–81 (1998)
3. Tyryshkin, K., Mousavi, P., Beek, M., Ellis, R., Dichora, P., Abolmaesumi, P.: A navigation system for shoulder arthroscopic surgery. Journal of Engineering in Medicine: Special Issue on Navigation Systems in Computer-assisted Orthopaedic Surgery, 801–812 (2007)
4. Hacihaliloglu, I., Abugharbieh, R., Hodgson, A., Rohling, R.: Bone Surface Localization in Ultrasound Using Image Phase Based Features. Ultrasound in Med. and Biol. 35(9), 1475–1487 (2009)
5. Penney, G.P., Edwards, P.J., King, A.P., Blackall, J.M., Batchelor, P.G., Hawkes, D.J.: A Stochastic Iterative Closest Point Algorithm (stochastICP). In: Niessen, W.J., Viergever, M.A. (eds.) MICCAI 2001. LNCS, vol. 2208, pp. 762–769. Springer, Heidelberg (2001)
6. Moghari, M.H., Abolmaesumi, P.: Point-Based Rigid-Body Registration Using an Unscented Kalman Filter. IEEE Transactions on Medical Imaging 26(12), 1708–1728 (2007)
7. Brounstein, A., Hacihaliloglu, I., Guy, P., Hodgson, A., Abugharbieh, R.: Towards Real-Time 3D US to CT Bone Image Registration Using Phase and Curvature Feature Based GMM Matching. In: Fichtinger, G., Martel, A., Peters, T. (eds.) MICCAI 2011, Part I. LNCS, vol. 6891, pp. 235–242. Springer, Heidelberg (2011)
8. Brendel, B., Winter, S., Rick, A., Stockheim, M., Ermert, H.: Registration of 3D CT and Ultrasound Datasets of the Spine Using Bone Structures. Computer Aided Surgery 7, 146–155 (2002)
9. Penney, G., Barratt, D., Chan, C., Slomczykowski, M., Carter, T., Edwards, P., Hawkes, D.: Cadaver Validation of Intensity-Based Ultrasound to CT Registration. Medical Image Analysis 10(3), 385–395 (2006)
10. Gill, S., Abolmaesumi, P., Fichtinger, G., Boisvert, J., Pichora, D., Borshneck, D., Mousavi, P.: Biomechanically Constrained Groupwise Ultrasound to CT Registration of the Lumbar Spine. Medical Image Analysis (2010) (in Press)
11. Khallaghi, S., Mousavi, P., Borschneck, D., Fichtinger, G., Abolmaesumi, P.: Biomechanically Constrained Groupwise Statistical Shape Model to Ultrasound Registration of the Lumbar Spine. In: Taylor, R.H., Yang, G.-Z. (eds.) IPCAI 2011. LNCS, vol. 6689, pp. 47–54. Springer, Heidelberg (2011)
12. Foroughi, P., Boctor, E., Swatrz, M.J., Taylor, R.H., Fichtinger, G.: Ultrasound bone segmentation using dynamic programming. In: IEEE Ultrasonics Syposium, pp. 2523–2526 (2007)
13. Hacihaliloglu, I., Abugharbieh, R., Hodgson, A.J., Rohling, R.: Automatic Bone Localization and Fracture Detection from Volumetric Ultrasound Images Using 3D Local Phase Features. Ultrasound in Medicine and Biology 38(1), 128–144 (2011)
14. Tsuboi, T., Hirai, S.: Detection of Planar Motion Objects Using Radon Transform and One-Dimensional Phase-Only Matched Filtering. Systems and Computers in Japan 37(5), 1963–1972 (2006)
15. Gurbuz, A.C., McClellan, J.H., Romberg, J., Scott, W.R.: Compressive sensing of parameterized shapes in images. In: Proceedings of IEEE International Conference on Acoustics, Speech and Signal Processing, pp. 1949–1952 (2008)